520

521 *Geophysical Research Letters*

522 Supporting Information for

523 **Major modes of climate variability dominate nonlinear Antarctic ice-sheet elevation changes 2002-**
524 **2020**

525 Matt A. King[1,2], Poul Christoffersen[2,3]

526 [1]School of Geography, Planning, and Spatial Sciences, University of Tasmania, Hobart, Tasmania
527 7001, Australia

528 [2]The Australian Centre for Excellence in Antarctic Science, University of Tasmania, Hobart,
529 Tasmania 7001, Australia

530 [3]Institute for Marine and Antarctic Studies, University of Tasmania, Hobart, Tasmania 7001,
531 Australia

532

533

534 **Contents of this file**

535

536 Text S1
537 Figures S1 to S9
538 Table S1

539

540

Text S1

To make a first-order estimate of plausible velocity-driven changes on surface elevation on Pine Island and Thwaites Glacier, we used annual Measures v2 ice velocities (Rignot et al., 2017) to derive year-on-year velocity changes at the glacier point positions where we extracted time series of surface elevation changes (shown in Fig. 3). The annual velocity changes were extracted in polar stereographic coordinates (x, y) and averaged over a 25 × 25 km box centred around each of the two geographical locations. The corresponding changes in surface height were estimated from the conservation of mass:

$$\frac{\partial h}{\partial t} = \dot{a} + \dot{b} + \bar{v} \cdot \nabla \mathrm{H} + \mathrm{H} \cdot \dot{\varepsilon}_z$$

where $\dot{a}$ is the surface accumulation from snowfall, $\dot{b}$ is the basal accumulation when water at the bed freezes on (negative for melting), $\bar{v}$ is the velocity vector, ∇ is the gradient operator, H is ice thickness and $\dot{\varepsilon}_z$ is the vertical stain rate averaged for the ice column. We used the third and fourth term on the RHS to derive estimates of the elevation change stemming specifically from the change in velocity, ignoring the accumulation terms $\dot{a}$ and $\dot{b}$. If the velocity change is $\delta\bar{v}$, the change in height is $-\delta\bar{v} \cdot \nabla \mathrm{H} + \mathrm{H} \cdot \delta\dot{\varepsilon}_z$, where the first term denotes elevation gain from advection of thicker ice (or the opposite) and the second term is elevation loss due to dynamic thinning when the ice velocity increases (or the opposite). The change in velocity, $\delta\bar{v} = (\Delta v_x, \Delta v_y)$ was the annual difference from one year to the next. The advection term was calculated as $\Delta v_x \, dh/dx + \Delta v_y \, dh/dy$, while strain thinning was calculated as $\mathrm{H}(-\Delta(dv_x/dx) - \Delta(dv_y/dy))$ with the assumption that ice is incompressible ($\delta\dot{\varepsilon}_z = -\delta\dot{\varepsilon}_x - \delta\dot{\varepsilon}_y$) and vertical strain in the ice column is uniform. Fig. S10 shows the estimated elevation change in terms of advection and strain and their total.

Supplementary Figures

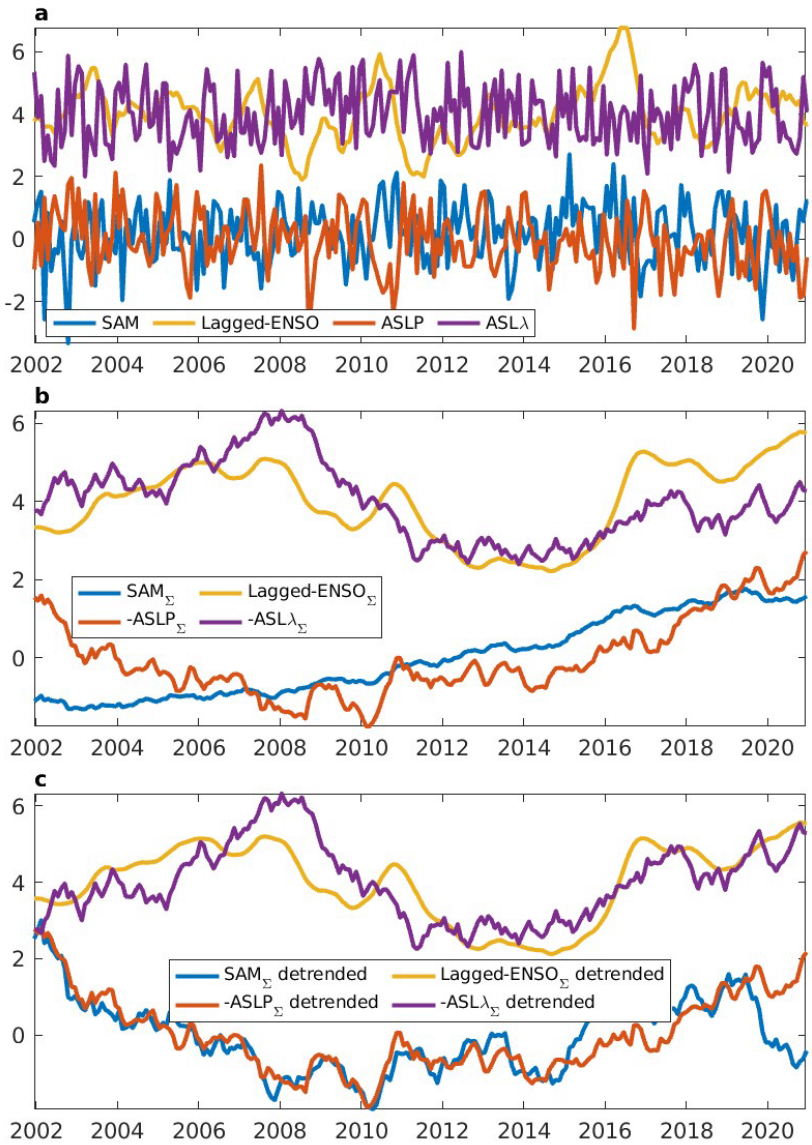

Fig S1. Cumulatively summed and detrended climate indices. The panels show the normalized climate indices (a), their cumulative sum renormalized (b), after further detrending and renormalization (c). ENSO and ASLλ terms are shown offset by 4 units for clarity.

576

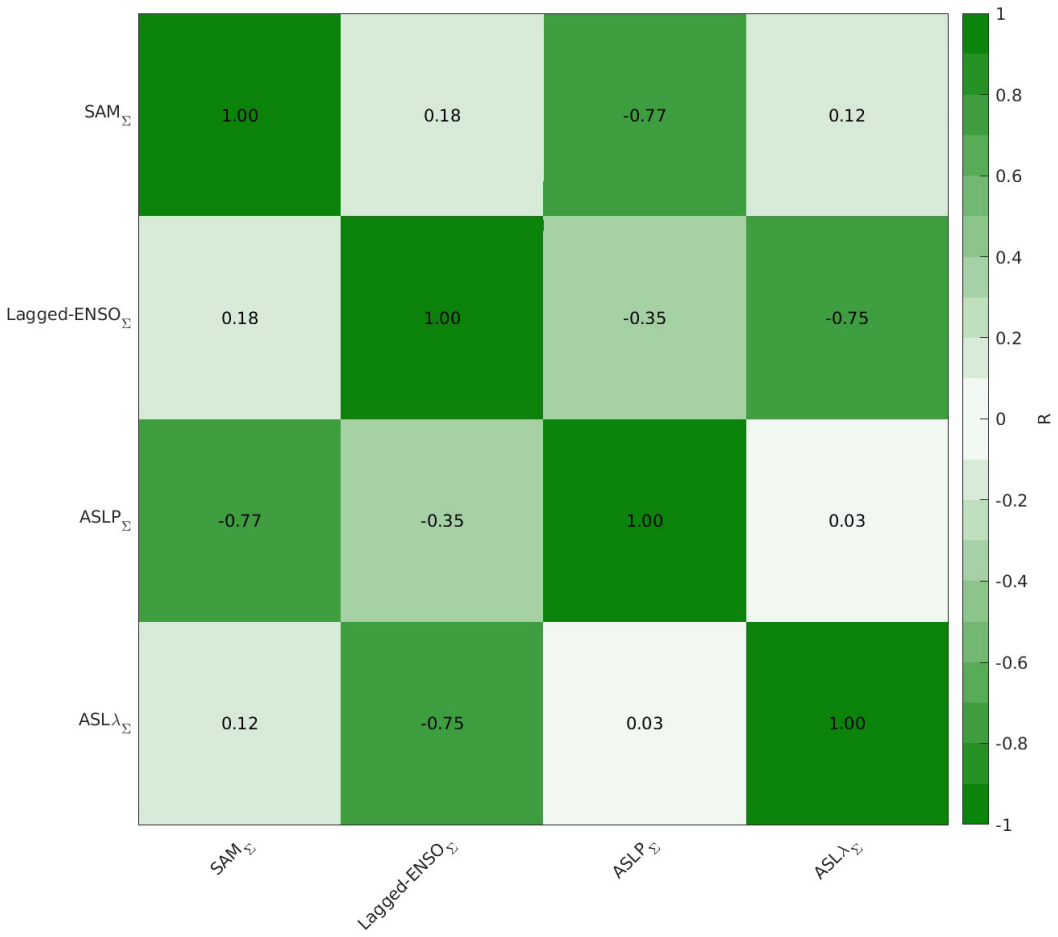

577
578
579 **Fig S2.** Correlation coefficients of summed and detrended climate indices.
580

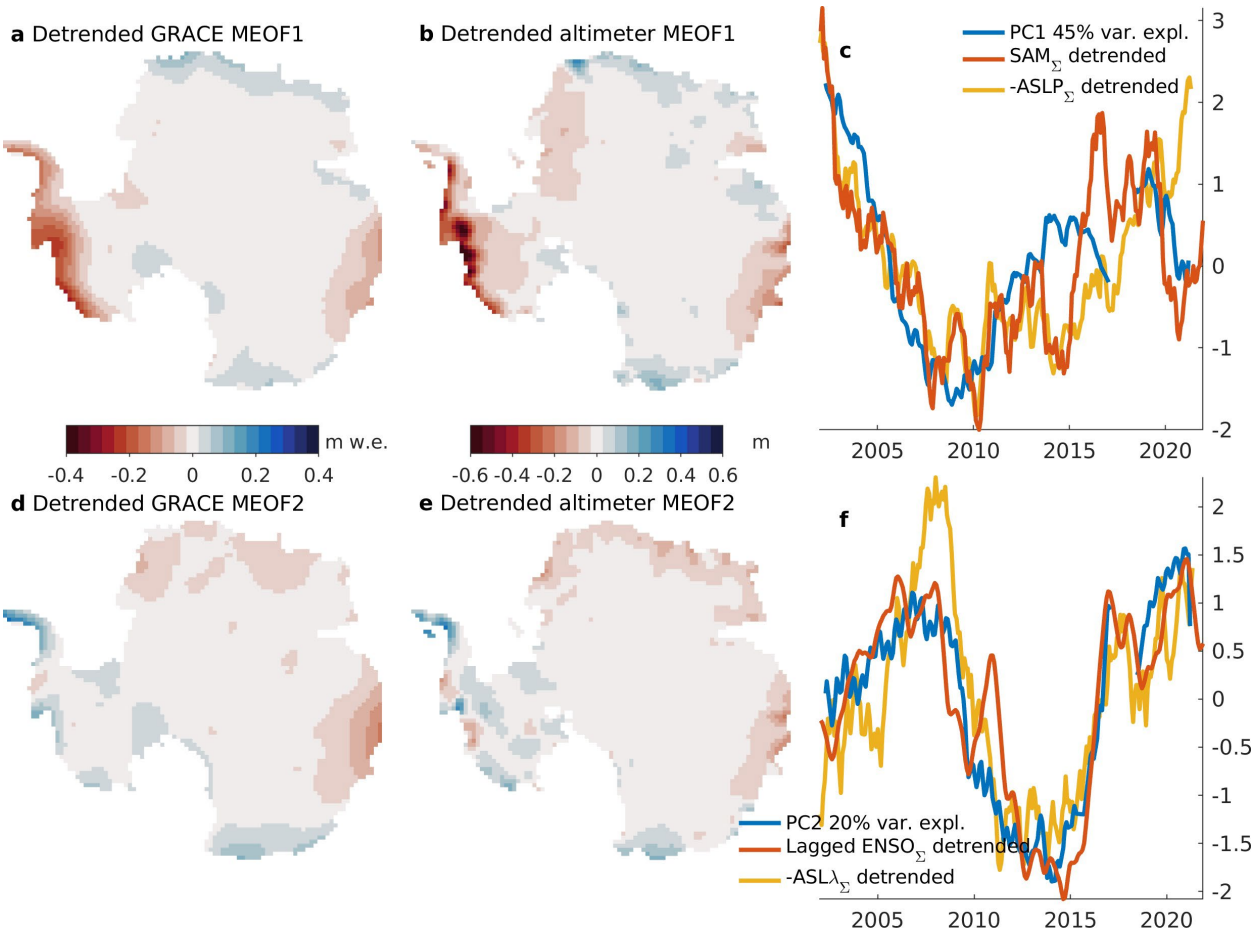

Fig S3. The leading two modes of the detrended altimeter and GRACE data based on MVEOF. The EOFs are shown after scaling to reverse the effects of normalization. GRACE modes (a, d) are shown in units of meters of water equivalent (w.e.), and altimeter modes (b, e) shown in units of meters of ice elevation. Overlain on PC1 is the detrended SAM_Σ and $-ASLP_\Sigma$ indices and overlain on PC2 is the lagged $ENSO_\Sigma$ and $-ASL\lambda_\Sigma$. The variances explained by each mode are indicated in the legends of panels c and f.

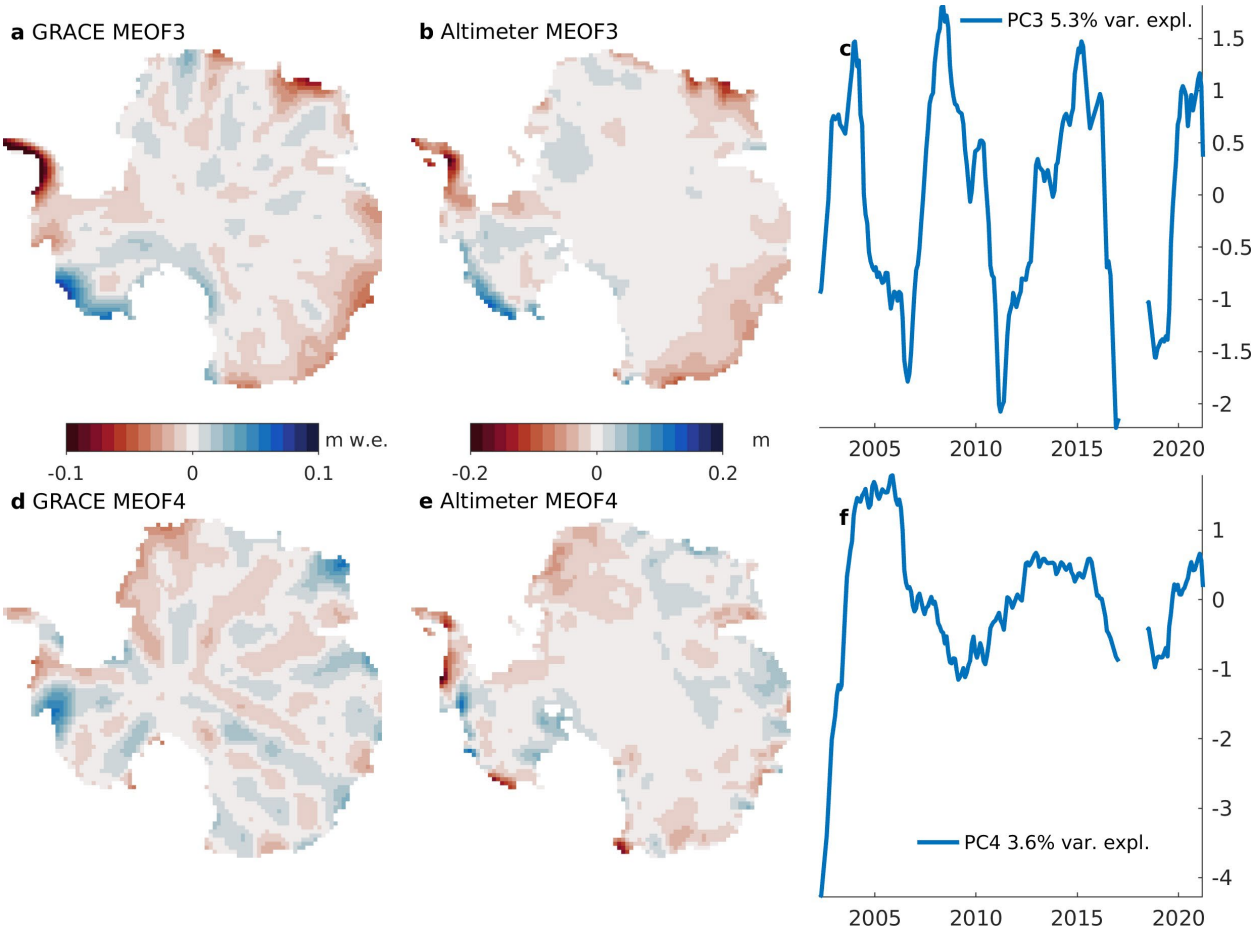

Fig S4. Modes 3 and 4 of the MVEOF. Note the changes in color scale from Fig S3.

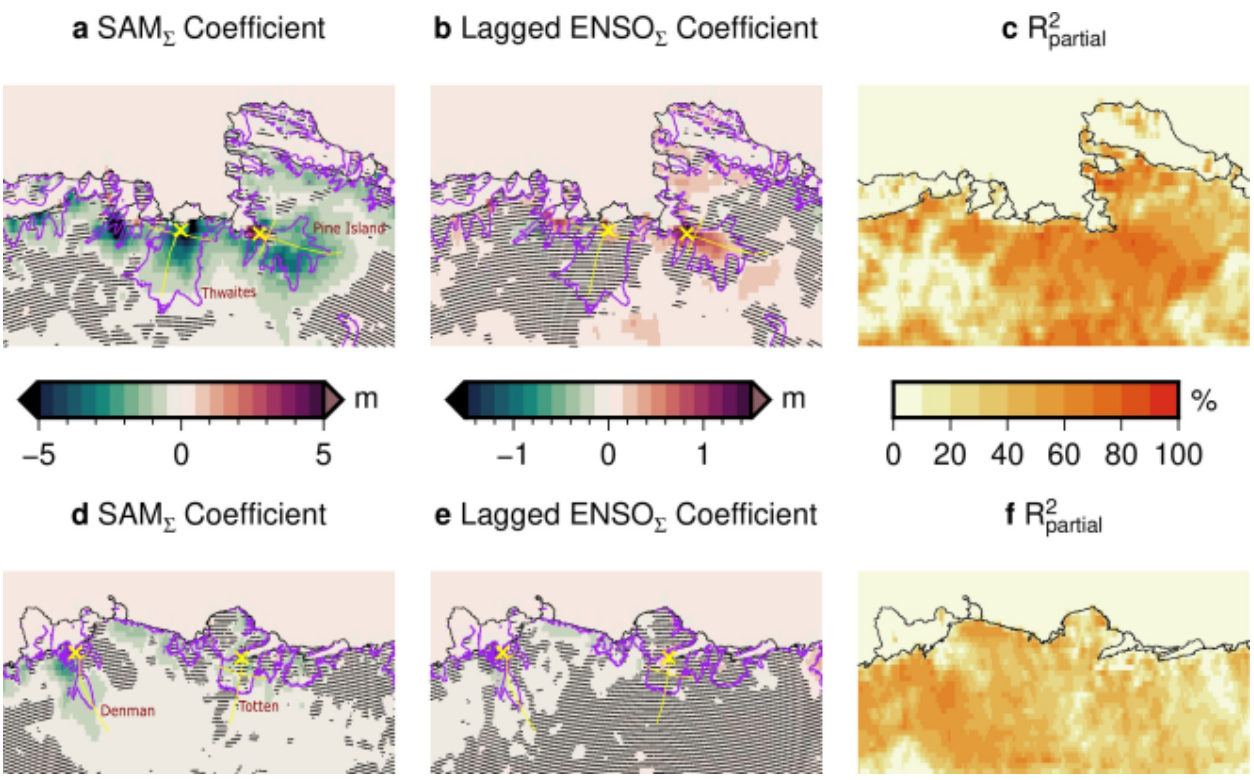

Fig S5. Detail of Figure 1 in the Amundsen Sea Embayment (top) and Denman-Totten glacier (bottom) regions. Thick black lines show the grounding line and thin black lines the ice shelf limits (Haran et al., 2014, updated 2019). Pink lines define the 100 m/yr speed contour (Rignot et al., 2017). Yellow lines mark the locations of ice stream profiles and yellow cross marks the location of the ice stream time series.

606
607

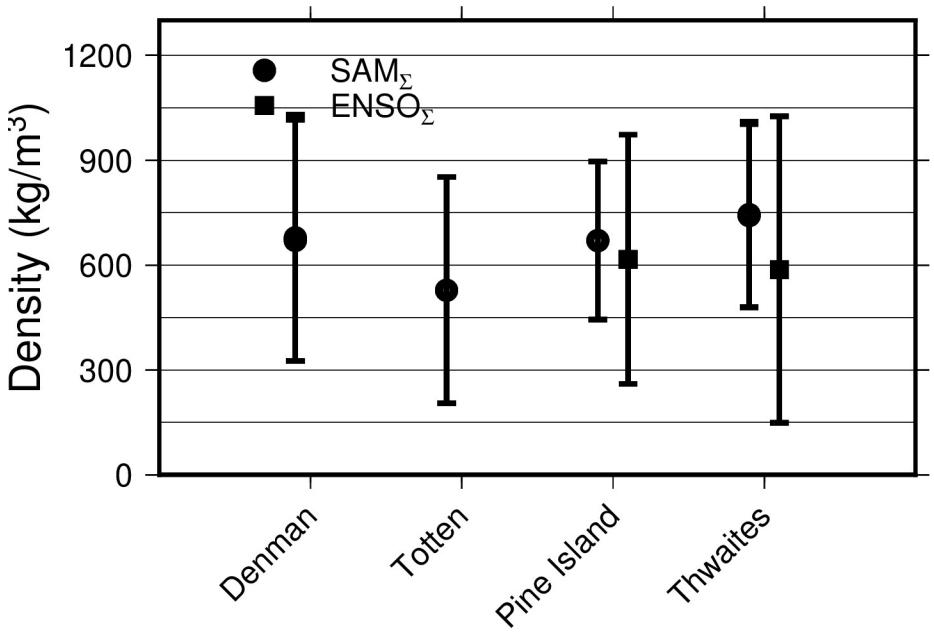

608
609
610 **Fig S6.** Density of SAM_{Σ} and $ENSO_{\Sigma}$ variability from the ratio of GRACE and smoothed-
611 altimetry coefficients. Error bars reflect 1-sigma uncertainties. $ENSO_{\Sigma}$ values are not
612 shown for Denman and Totten as they are too uncertain.
613

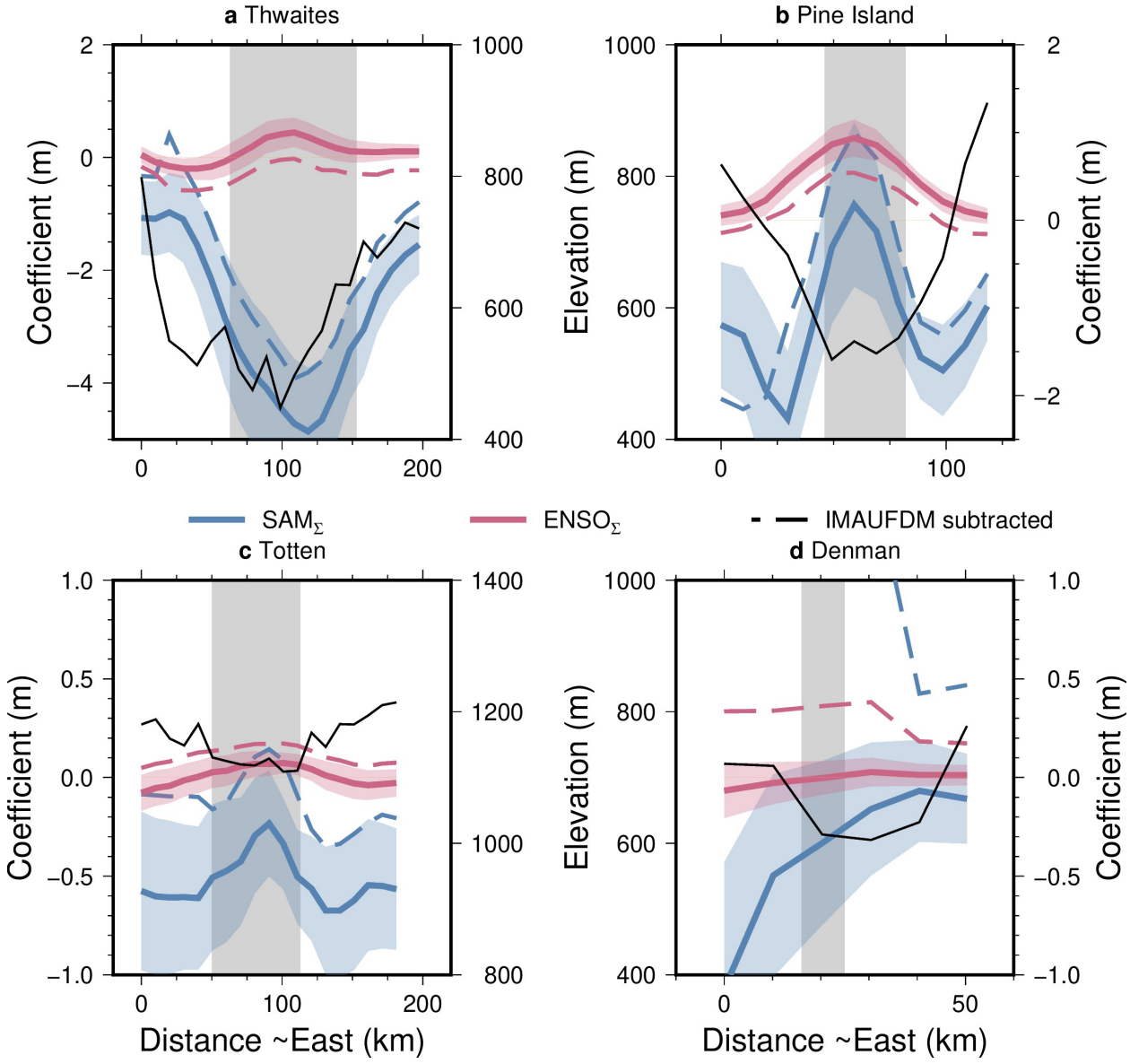

Fig S7. Cross-section profiles of SAM$_\Sigma$ (a) and ENSO$_\Sigma$ (b) coefficients as a function of distance across Thwaites (a), Pine Island (b), Totten (c) and Denman (d) glaciers. Coefficients are shown as estimated before (colored solid line) and after (colored dashed line) subtraction of the IMAU FDM. The ice elevation extracted from the REMA v2.0 1 km mosaic (Howat, 2022) is shown as a black line (central axes). Colored shading indicates the 1-sigma confidence limits. The vertical grey box indicates the 100 m/yr limits of ice flow based on Measures v2. The locations of the profiles are shown in Figure S5 as yellow lines.

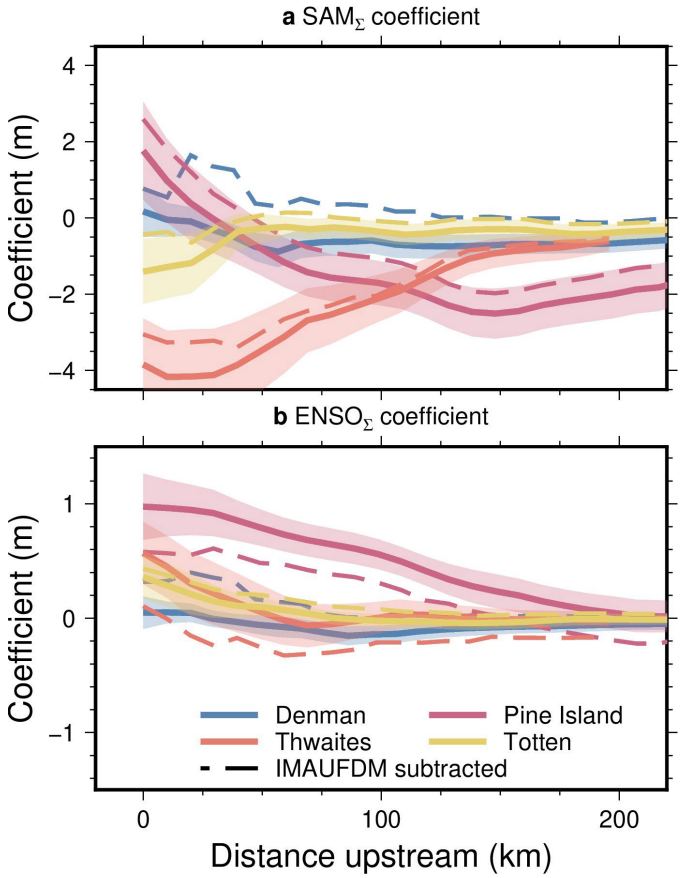

Fig S8. Centre-line profiles of SAM$_\Sigma$ (a) and ENSO$_\Sigma$ (b) coefficients as a function of distance upstream of the grounding line of major ice streams. Coefficients are shown before (solid line) and after (dashed line) subtraction of the IMAU FDM. Shading indicates the 1-sigma confidence limits. The locations of the profiles are shown in Figure S5 as yellow lines.

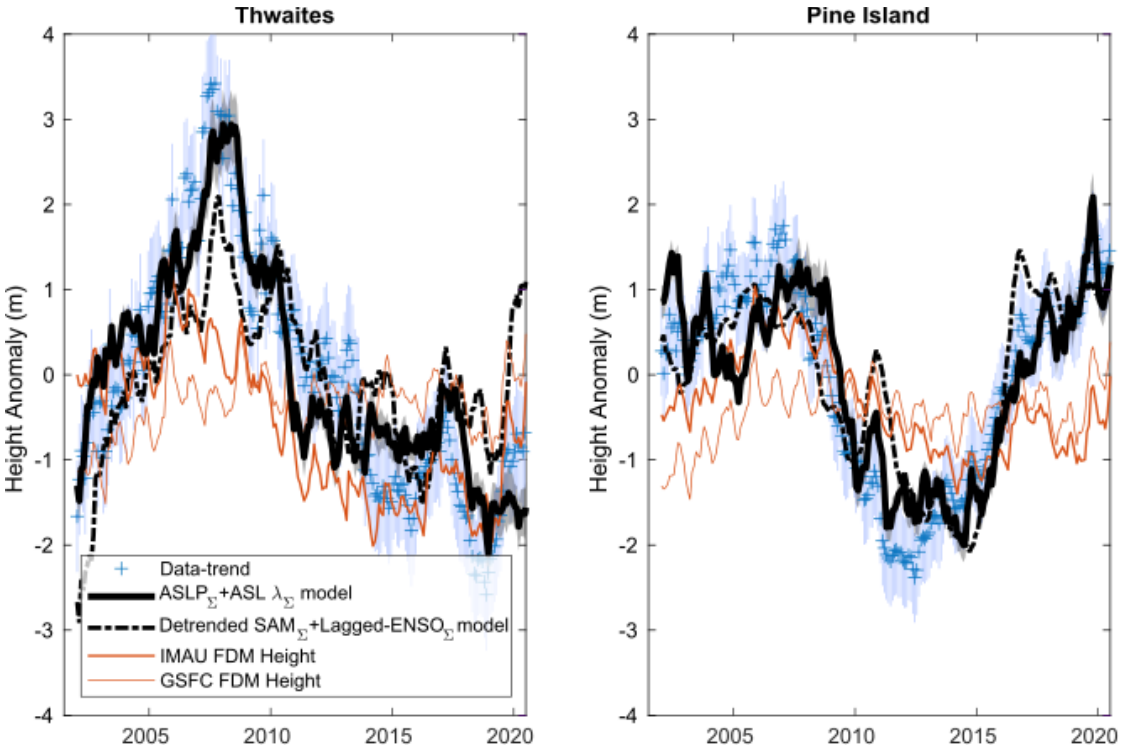

Figure S9. As for Figure 3 but showing only the Thwaites and Pine Island time series. Panels show (left axes) the detrended data and their 2-sigma uncertainties (blue plusses and error bars), outputs of two models of firn densification (FDM; brown lines), the best fitting models based on ASL (black solid line with 2-sigma uncertainty in gray shading) and SAM+ENSO (black dashed lines) terms.

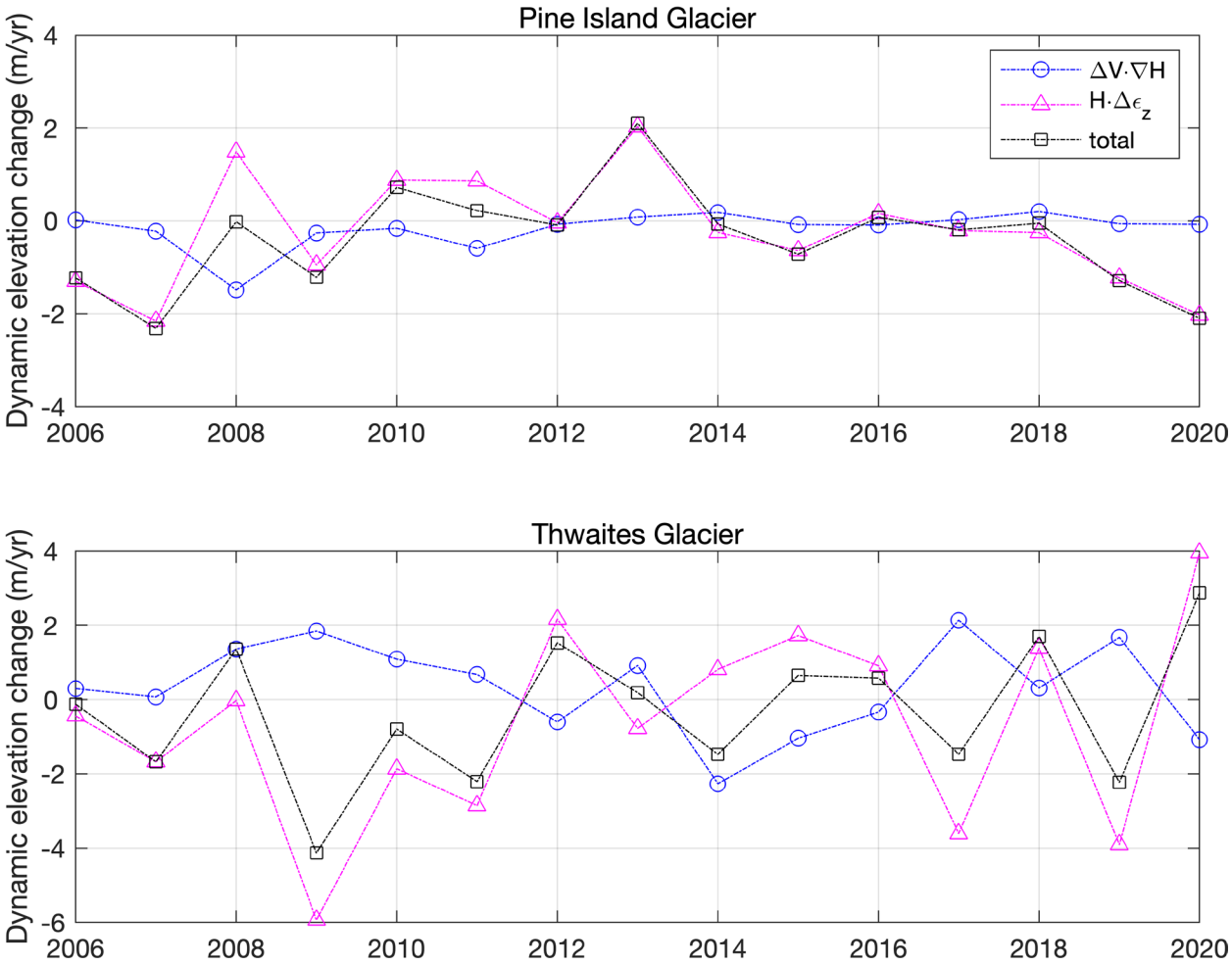

Figure S10. Dynamic elevation change anomalies (positive for gain) estimated from annual changes in satellite derived velocities for Pine Island Glacier (top) and Thwaites Glacier (bottom). These elevation change anomalies are calculated from the advective thickness change (blue circles) and strain (magenta triangle) tied to the observed change in velocity from one year to the next. The total elevation change (black squares) is the sum. Estimates are based on gridded surface velocities (v_x, v_y) in a 25 x 25 km box centered around glacier points used to show observed elevation changes in Figure 3 of main text. Other sources of elevation change are ignored. See Text S1 for details.

652

653 Table S1

654

655 Table S1. Location in Antarctic Polar Stereographic coordinates (EPSG:3031) of sites in Fig. 3
656 and Fig S9 and discussed in the main text.

Glacier	**X(m)**	**Y(m)**
Thwaites	-1511702	-463473
Pine Island	-1583860	-232513
Totten	2274795	-988293
Denman	2496950	-423352

657